

## A Case Study of Complex Metallic Alloy Phases: Stability, Structure and Disorder Phenomena of Mg-Pd and Ag-Mg Compounds

Julien P. A. Makongo, Christian Kudla, Yurii Prots, Ulrich Burkhardt, Andreas Leineweber<sup>1</sup>, Rainer Niewa<sup>2</sup>, and Guido Kreiner

Complexity in the sense of giant unit cells and inherent structural disorder is one of the most pronounced features of complex metallic alloy phases (CMAs). Prominent examples of CMAs are approximant phases of icosahedral quasicrystals with the Mackay icosahedron as fundamental structural unit. In order to achieve a deeper insight into the relation between the homogeneity ranges, crystal structures and disorder phenomena of CMA phases the Mg-Pd [1-4] and the Ag-Mg [5-7] system have been re-determined. Six novel Mg-rich phases have been discovered during the investigations. Two examples,  $\beta$ -Mg<sub>6</sub>Pd and  $\gamma$ -AgMg<sub>4</sub>, will be discussed in the following sections in order to show structural complexity including inherent disorder.

The Mg-Pd system contains the following intermediate phases: Mg<sub>6</sub>Pd ( $\beta$ , [8]), Mg<sub>57</sub>Pd<sub>13</sub> ( $\gamma$ , [1]), Mg<sub>56.4</sub>Pd<sub>13.5</sub> ( $\delta$ , [1]), Mg<sub>306</sub>Pd<sub>77</sub> ( $\epsilon$ , [9]), Mg<sub>78.5</sub>Pd<sub>21.5</sub> ( $\xi$ , [1]), Mg<sub>3</sub>Pd ( $\eta$ , [2]), Mg<sub>5</sub>Pd<sub>2</sub> ( $\theta$ , [10]), Mg<sub>2</sub>Pd ( $\iota$ , [3]), MgPd ( $\kappa$ , [10]), Mg<sub>0.9</sub>Pd<sub>1.1</sub> ( $\lambda$ , [11]), Mg<sub>3</sub>Pd<sub>5</sub> ( $\mu$ , [12]), MgPd<sub>2</sub> ( $\nu$ , [12]), and MgPd<sub>3</sub> ( $\xi$ , [12]). The intermetallic compounds  $\beta$  to  $\xi$  are CMAs of the

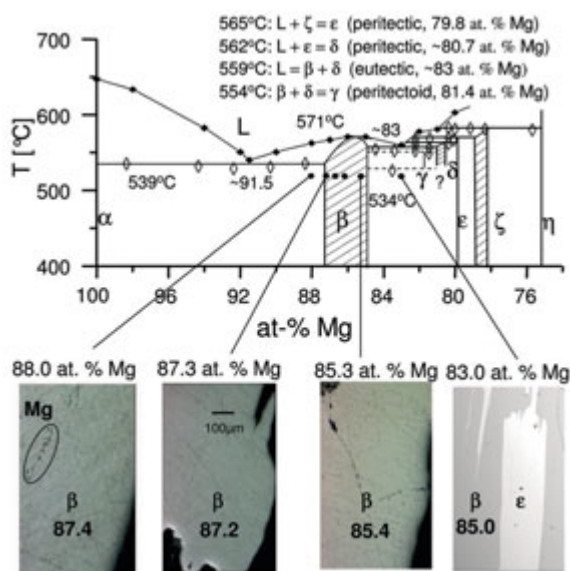


Fig. 1: Mg-rich part (100 – 75 at. % Mg) of the Mg-Pd phase diagram. The microstructures of four alloys annealed at 530 °C covering the homogeneity range of the  $\beta$  phase are shown for clarity.

Mackay icosahedron type with giant unit cells containing several hundred atoms. The  $\beta$  phase melts congruently and crystallizes within a narrow phase field while  $\gamma$ ,  $\delta$ ,  $\epsilon$  and  $\xi$  form (Fig. 1) in a cascade of peritectoid and peritectic reactions in a small temperature ( $\sim 30$  °C) and composition range ( $\sim 3$  at.%). The accumulation of CMAs within such a narrow composition range strongly suggests the stability of the Mackay icosahedra as fundamental structural units, since the composition of the cluster is fixed. A small change in the phase composition of about 1 at.% corresponds to a change of approximately 5 – 10 at.% in the regions between the Mackay icosahedra, causing a different kind of cluster packing. Thus, the accumulation of CMAs in regions of the phase diagram with nearly equal composition is plausible.

The  $\beta$  phase Mg<sub>6</sub>Pd is of a different nature since the Mackay icosahedra are highly disordered giving rise to a homogeneity range. Mg<sub>6</sub>Pd crystallizes in a large face-centred cubic unit cell with space group  $F\bar{4}3m$  [8]. The unit cell parameter  $a$  decreases linearly from 20.1985(6) Å at the Mg-rich limit (Mg<sub>87.4(1)</sub>Pd<sub>12.6</sub>) to 20.045(5) Å at the Pd-rich limit (Mg<sub>85.0(1)</sub>Pd<sub>15.0</sub>). The crystal structure (Fig. 2) is conveniently described as an arrangement of inter-

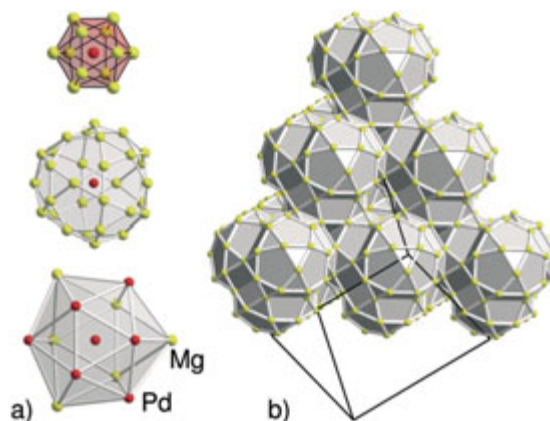


Fig. 2: The crystal structure of Mg<sub>6</sub>Pd. a) Concentric shell structure of the Mackay icosahedron. b) Packing of the Mackay icosahedra with interpenetrating and pentagonal face-sharing clusters.

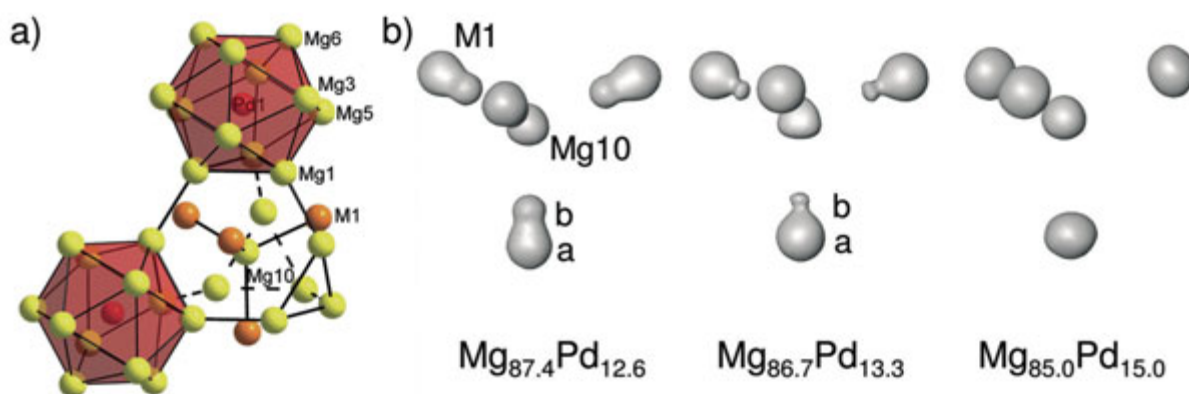


Fig. 3: The crystal structure of  $Mg_6Pd$ . a) Part of the crystal structure with inner icosahedra of the Mackay icosahedra forming a truncated tetrahedron. b) Isosurfaces of the electron density at M1 and Mg10 at various compositions of  $Mg_6Pd$ .

penetrating and pentagonal face-sharing distorted Mackay icosahedra. Four of the 14 crystallographic sites of  $Mg_6Pd$  are affected by disorder. The positions of the defect sites M1, Mg1, Mg5, and Mg10 are shown in Fig. 3a. The inner icosahedra of four Mackay icosahedra form truncated tetrahedra with Mg1 at the vertices. Here, for clarity, two of the icosahedra as well as all surrounding icosidodecahedral shells are omitted. A truncated tetrahedron is occupied at the centre by Mg10 and its hexagon faces are capped by M1. Mg5 is located at the vertices of the inner icosahedra adjacent to Mg1. Isosurfaces of the electron density ( $4 e/\text{\AA}^3$ ) obtained from X-ray single crystal structure refinements at M1 and Mg10 for  $Mg_6Pd$  at 87.4 at.%, 86.7 at.% and 85.0 at.% Mg are displayed in Fig. 3b. At the Mg-rich limit the Mg10 site is partially occupied and the M1 site reveals an electron density distribution corresponding to an atomic split position. M1a is occupied by Pd or Mg and M1b by Mg. A higher Pd content increases the observed electron densities at M1a (more Pd) and reduces the density at M1b (less Mg). Parallel, the electron density at Mg10 increases until the position is fully occupied by Mg, while constitutional vacancies appear at the Mg1 site in combination with a large anisotropic displacement of Mg5. Finally, at the Pd-rich limit the electron density at M1b disappears and M1a is occupied by approximately 2/3 Pd and 1/3 Mg.

An interpretation in terms of crystal chemistry of the observed electron density at the defect sites of  $Mg_6Pd$  is as follows. At the Pd-rich phase boundary the atomic environment of Mg10 is a Frank-Kasper Z16 coordination type polyhedron with a maximum of two vacancies at the Mg1 positions (Fig. 4a).

The centre of the Z16 is fully occupied by Mg whereas the hexagon caps are randomly occupied by Pd or Mg. The M1 site is at maximum surrounded by 13 Mg atoms (Fig. 4b). In case of Pd at M1 the coordination number is 12 due to a vacancy at one of the Mg1 neighbours. In that case the displacement of the Mg5 neighbours shortens the interatomic distances to the central Pd atom. A vacancy at the Mg1 position creates a truncated inner icosahedron whereas the icosidodecahedral shell is modified by inserting the Mg10 atom slightly above a triangular face (Fig. 4c). With increasing Mg content the M1a site becomes richer in Mg reducing the number of vacancies at Mg1 positions and the number of displaced Mg5 atoms. However, part of the excess Mg additionally occupies the M1b site. In that case a simultaneous occupation of M1a or Mg10 is forbidden since the interatomic dis-

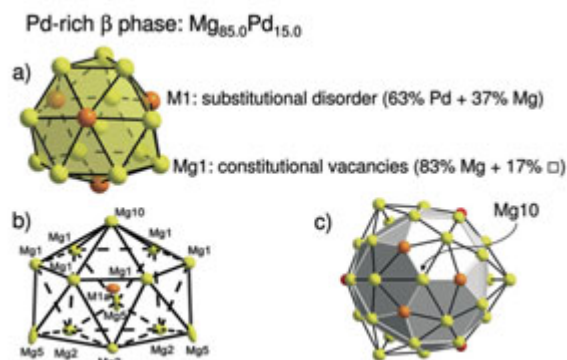


Fig. 4: The crystal structure of  $Mg_6Pd$ . Interpretation of the electron density for the Pd-rich phase. a) Z16 polyhedron surrounding the Mg10 site. b) Coordination type polyhedron for M1. c) Mackay icosahedron with one additional Mg atom.

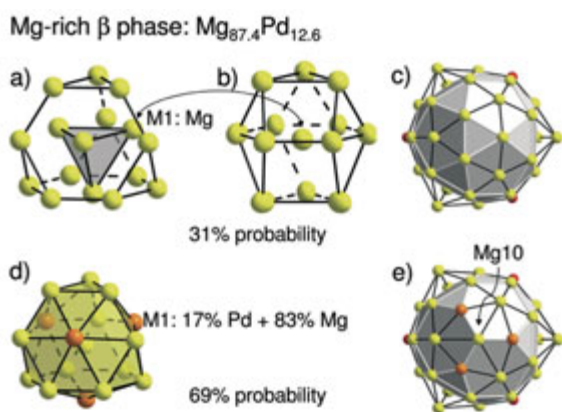


Fig. 5: The crystal structure of  $\text{Mg}_6\text{Pd}$ . Interpretation of the electron density for the Mg-rich phase. a) A truncated tetrahedron filled with a  $\text{Mg}_4$  tetrahedron replaces the Z16 polyhedron with 31% probability. b) Coordination type polyhedron for M1. c) Mackay icosahedron. d) Z16 polyhedron with 69% probability surrounding the Mg10 site. e) Mackay icosahedron with an additional Mg10 at a local threefold axis.

tances are too small. Here, a likely scenario is the simultaneous occupation (Fig. 5a) of the four M1b positions by Mg per truncated tetrahedron. The truncated tetrahedron of Mg1 atoms together with the inner  $\text{Mg}_4$  tetrahedron forms a new structural unit. Moreover, the icosidodecahedral shells (Fig. 5c) of the surrounding Mackay icosahedra are in that case nearly perfect. The coordination type polyhedron of Mg at M1b is then an anti-cuboctahedron (Fig. 5b) formed by 12 Mg atoms. From a geometrical point of view the occupation of Mg at M1b seems to be the natural decoration for  $\text{Mg}_6\text{Pd}$  resulting in the formula  $\text{Mg}_{43}\text{Pd}_6$  ( $Z = 8$ , 87.8 at.% Mg). However, in the crystal structure of Mg-rich  $\text{Mg}_6\text{Pd}$  only 31% of the truncated tetrahedra are decorated with  $\text{Mg}_4$  tetrahedra while the remaining 69% are filled with  $(\text{Pd}_x\text{Mg}_{1-x})_4\text{Mg}$  units (Fig. 5d,e).

The Ag-Mg system contains three complex metallic alloys phases:  $\text{Ag}_{7+x}\text{Mg}_{26-x}$  ( $\epsilon$ , [13]),  $\text{Ag}_{17}\text{Mg}_{54}$  ( $\epsilon'$ , [14]) and  $\gamma$ - $\text{AgMg}_4$  ( $\gamma$ , [5, 7]). The crystal structures of  $\epsilon$  and  $\epsilon'$  are best described as *fcc* ( $\epsilon$ ) and *bcc* ( $\epsilon'$ ) packings of Mackay icosahedra composed of 13 Ag + 42 Mg atoms. The  $\epsilon'$  phase is a high temperature phase of  $\epsilon$ . Both have a narrow homogeneity range of about 2.5 at.% mainly due to substitutional disorder in the regions between the Mackay icosahedra. The  $\gamma$  phase is structurally different to  $\epsilon$  and  $\epsilon'$ , since the crystal structure does not contain Mackay icosahedra. It forms peritectoidically ( $\gamma = \epsilon + \text{Mg}(\text{Ag})$ ) at 472(2) °C without homogeneity range at 80.34(6) at.% Mg. However, its

crystal structure ( $\text{Ag}_{9.01(3)}\text{Mg}_{36.81(6)}$ ,  $Z = 2$ ,  $P6_3/m$ ,  $a = 12.4852(8)$  Å,  $c = 14.4117(9)$  Å) reveals an intricate pattern of inherent configurational disorder.

A hypothetical crystal structure of  $\gamma$  (Fig. 6) without disorder corresponds to the composition  $\text{Ag}_9\text{Mg}_{37}$  (80.43 at.% Mg). Here, most Ag atoms are icosahedrally surrounded and form a packing of vertex sharing and interpenetrating icosahedra (Fig. 6a) with the remaining space filled by an alternate sequence of distorted Mg centred icosahedra and Ag centred tri-capped trigonal prisms (Fig. 6b) running along [001]. However, the  $\gamma$  phase is inherently disordered. The electron density distribution enclosing  $(0, 0, z)$  is shown in Fig. 7a. The corresponding model in Fig. 7b roughly defines two Z15 polyhedra per unit cell. The split positions (Mg2, Ag1) and (Mg6, Ag2) occupy vertices of Z15 while Mg9 ( $z = 0.12, 0.38, 0.62, 0.88$ ), Ag5 ( $z = 0.19, 0.31, 0.69, 0.81$ ) and Mg10 ( $z = 0.25, 0.75$ ) inside Z15 are partially occupied. There are four simple solutions for a string of atoms along [001]

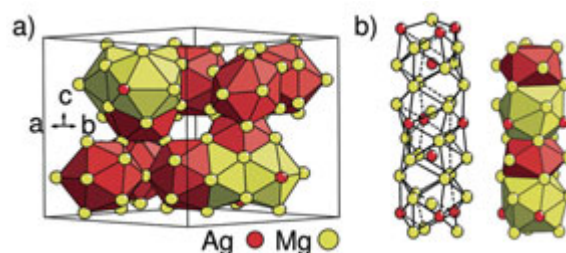


Fig. 6: A hypothetical crystal structure for the composition  $\text{Ag}_9\text{Mg}_{37}$ . The red and yellow polyhedra are centred by Ag and Mg atoms, respectively. a) Icosahedral network of vertex connected and interpenetrating icosahedra. b) The alternate stacking of distorted icosahedra and tri-capped trigonal prisms along [001] with the polyhedra centred at  $0, 0, z$ .

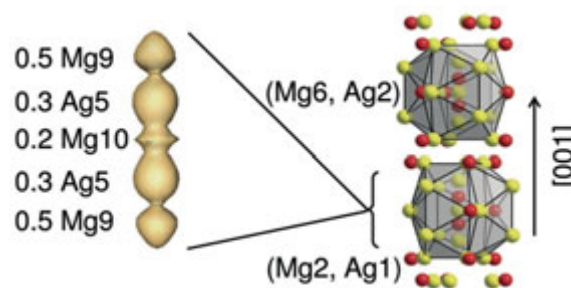


Fig. 7: The crystal structure of  $\gamma$ - $\text{AgMg}_4$ . The split atom model roughly forms two Z15 polyhedra per unit cell. The isosurface of the electron density inside a Z15 polyhedron is shown together with the site occupancy of the respective density maxima.

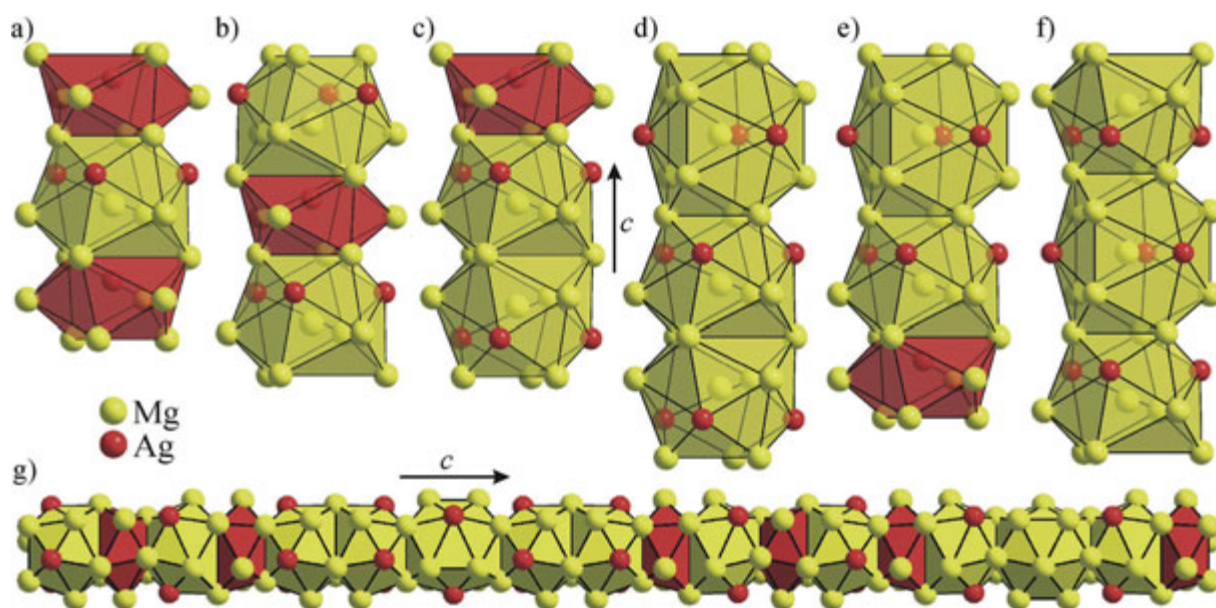


Fig. 8: The crystal structure of  $\gamma$ -AgMg<sub>4</sub>. Local sequences of polyhedra are shown which are compatible with the local distance constraints. The polyhedra stack along [001] with centres at 0, 0, z. a) (Ag5–Mg9–Ag5); b) (Mg9–Ag5–Mg9); c) (Ag5–Mg9–Mg9); d) (Mg10–Mg9–Mg9); e) (Mg10–Mg9–Ag5); f) (Mg9–Mg10–Mg9); g) Sequence of polyhedra with  $c' = 5c$ .

avoiding short distances and being compatible with the observed translational symmetry:

$$A(\uparrow) = |\text{Mg9}(0.12)\text{--Ag5}(0.31)\text{--Mg9}(0.62)\text{--Ag5}(0.81)|$$

$$B(\uparrow) = |\text{Mg9}(0.12)\text{--Mg9}(0.38)\text{--Mg10}(0.75)|$$

$$A(\downarrow) = |\text{Ag5}(0.19)\text{--Mg9}(0.38)\text{--Ag5}(0.69)\text{--Mg9}(0.88)|$$

$$B(\downarrow) = |\text{Mg10}(0.25)\text{--Mg9}(0.62)\text{--Mg9}(0.88)|$$

Solutions up ( $\uparrow$ ) and down ( $\downarrow$ ) for A and B are related by inversion symmetry, respectively, and the numbers given in parentheses correspond to the z value. The solutions A correspond to the ordered model Ag<sub>9</sub>Mg<sub>37</sub> with space group  $P6_3$ . Solutions B describe a model structure in  $P3$  with a content of 79.12 to 82.42 at.% Mg depending on the occupation of the split atom position (Mg6, Ag2) with Ag or Mg. Neither model A nor model B is stable at temperatures above 400 °C. The crystal structure reveals a random stacking of polyhedra along [001]. Random or ordered distributions of Mg9, Ag5 and Mg10 with site occupancy factors s.o.f.(Mg9) = 0.5, s.o.f.(Ag5) = x and s.o.f.(Mg10) = 0.5–x may be obtained by stacking their coordination polyhedra along [001] with the appropriate frequency. If N is the number of unit cells along c per domain or supercell then 2·N, 4·N·x and (1–2x)N are the numbers of Mg9, Ag5 and Mg10 polyhedra, respectively. The following substrings are compatible with the local distance constraints: (Ag5–Mg9–Ag5), (Mg9–Ag5–Mg9), (Ag5–Mg9–Mg9), (Mg10–Mg9–Ag9),

(Mg10–Mg9–Ag5), (Mg9–Mg10–Mg9). They are shown in Fig. 8 together with a sequence of polyhedra corresponding to a supercell with  $c' = 5c$  with space group  $P3$ . The latter sequence is a fairly good approximation of the random stacking of polyhedra as found in the crystal structure. Recent investigations using melt-spun alloys subsequently long-term annealed at 250 °C indicate the formation of an ordered low-temperature phase.

In case of  $\gamma$ -AgMg<sub>4</sub> the observed configurational disorder at higher temperatures is plausible since the partition of space along 0,0,z into a sequence of polyhedra is geometrically ambiguous. It is more difficult to understand the pattern of disorder in  $\beta$ -Mg<sub>6</sub>Pd. Here, the reason may be the conflict to achieve both, an optimized packing of all atoms as well as an optimized cluster type.

## References

- [1] J. P. A. Makongo, Yu. Moguilnikov, C. Kudla, D. Grüner, M. Schäper and G. Kreiner; Mat. Res. Soc. Symp. Proc. **805** (2004) LL2.1.1.
- [2] J. P. A. Makongo, Yu. Prots, R. Niewa, U. Burkhardt and G. Kreiner; Z. Kristallogr. NCS **220(3)** (2005) 291.
- [3] J. P. A. Makongo, C. Kudla, Yu. Prots, R. Niewa, U. Burkhardt and G. Kreiner; Z. Kristallogr. NCS **220(3)** 289.

- [4] *J. P. A. Makongo, Yu. Prots, U. Burkhardt, R. Niewa, C. Kudla and G. Kreiner*, *Phil. Mag.* **86** (2006) 427.
- [5] *C. Kudla and G. Kreiner*, *Z. Kristallogr. (Supplement)* **21** (2004) 170.
- [6] *C. Kudla and G. Kreiner*, *Z. Anorg. Allg. Chem.* **630** (2004) 1739.
- [7] *C. Kudla, Yu. Prots, A. Leinweber and G. Kreiner*, *Z. Kristallogr.* **220** (2005) 102.
- [8] *S. Samson*, *Acta Crystallogr. B* **28** (1972) 936.
- [9] *G. Kreiner, M. Schäpers and S. Spiekermann*, in *Aperiodic 97*, M. de Boissieu, J.-L. Verger-Gaugry, R. Currat (eds.), World Scientific Publishing, Singapore 1997, p. 241.
- [10] *R. Ferro*, *J. Less-Common Met.* **1** (1959) 424.
- [11] *I. F. Kripyakevich and E. I. Gladyshevskii*, *Kristallografiya* **5** (1960) 552.
- [12] *C. Wannek and B. Harbrecht*, *J. Solid State Chem.* **159** (2001) 113.
- [13] *G. Kreiner and S. Spiekermann*, *Z. Anorg. Allg. Chem.* **627** (2001) 2460.
- [14] *A. V. Arakcheeva, O. G. Karpinskii and W. E. Klesnichenko*, *Sov. Phys. Crystallogr.* **33** (1988) 907.

<sup>1</sup> Max Planck Institute for Metals Research, Stuttgart, Germany

<sup>2</sup> Present address: TU München, München, Germany